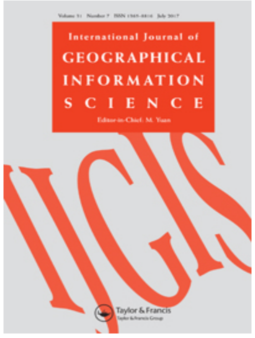

International Journal of Geographical Information Science

ISSN: 1365-8816 (Print) 1362-3087 (Online) Journal homepage: http://www.tandfonline.com/loi/tgis20

Safe separation distance score: a new metric for evaluating wildland firefighter safety zones using lidar

Michael J. Campbell, Philip E. Dennison & Bret W. Butler

INTERNATIONAL JOURNAL OF GEOGRAPHICAL INFORMATION SCIENCE, 2017
VOL. 31, NO. 7, 1448–1466
http://dx.doi.org/10.1080/13658816.2016.1270453

Taylor & Francis
Taylor & Francis Group

Safe separation distance score: a new metric for evaluating wildland firefighter safety zones using lidar

Michael J. Campbell[a], Philip E. Dennison[a] and Bret W. Butler[b]

[a]Department of Geography, University of Utah, Salt Lake City, UT, USA; [b]US Forest Service, Rocky Mountain Research Station, Missoula Fire Sciences Laboratory, Missoula, MT, USA

ABSTRACT

Safety zones are areas where firefighters can retreat to in order to avoid bodily harm when threatened by burnover or entrapment from wildland fire. At present, safety zones are primarily designated by firefighting personnel as part of daily fire management activities. Though critical to safety zone assessment, the effectiveness of this approach is inherently limited by the individual firefighter's or crew boss's ability to accurately and consistently interpret vegetation conditions, topography, and spatial characteristics of potential safety zones (e.g. area and geometry of a forest clearing). In order to facilitate the safety zone identification and characterization process, this study introduces a new metric for safety zone evaluation: the Safe Separation Distance Score (SSDS). The SSDS is a numerical representation of the relative suitability of a given area as a safety zone according to its size, geometry, and surrounding vegetation height. This paper describes an algorithm for calculating pixel-based and polygon-based SSDS from lidar data. SSDS is calculated for every potential safety zone within a lidar dataset covering Tahoe National Forest, California, USA. A total of 2367 potential safety zones with an SSDS ≥1 were mapped, representing areas that are suitable for fires burning in low wind and low slope conditions. The highest SSDS calculated within the study area was 9.65, a score that represents suitability in the highest wind-steepest slope conditions. Potential safety zones were clustered in space, with areas in the northern and eastern portions of the National Forest containing an abundance of safety zones while areas to the south and west were completely devoid of them. SSDS can be calculated for potential safety zones in advance of firefighting, and can allow firefighters to carefully compare and select safety zones based on their location, terrain, and wind conditions. This technique shows promise as a standard method for objectively identifying and ranking safety zones on a spatial basis.

ARTICLE HISTORY
Received 8 August 2016
Accepted 1 December 2016

KEYWORDS
Wildfire; firefighters; safety zones; lidar; GIS

1 Introduction

Between 1910 and 2015, there were 1087 documented wildland firefighter fatalities in the United States (National Interagency Fire Center 2016). The causes of fatalities vary greatly (Figure 1), but the leading causes fall into the category of burnovers,

CONTACT Michael J. Campbell mickey.campbell@geog.utah.edu

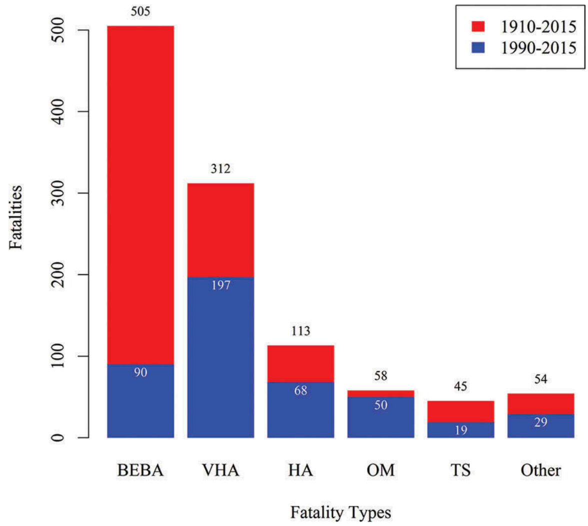

Figure 1. Wildland firefighter fatalities by type (BEBA = burnover, entrapment, burns, and asphyxiation; VHA = vehicle, helicopter, aircraft; HA = heart attack; OM = other medical; TS = tree, snag) (National Interagency Fire Center 2016).

entrapments, burns and asphyxiation (BEBA). BEBA are the direct result of fatal exposure to excessive heat, fire, and/or smoke and comprise 45% of the total fatalities from 1910 to 2015. Burnover results from fire rapidly overtaking firefighting personnel before they can move to a safe area, and entrapment indicates that firefighters' ability to move to a safe area is compromised. Though BEBA have declined as a percentage of total fatalities in recent decades (Figure 1), burnover and entrapment have been implicated in recent tragic incidents involving multiple fatalities, including 14 firefighters in the 1994 South Canyon fire in Colorado and 19 firefighters in the 2013 Yarnell Hill fire in Arizona (Butler *et al*. 1998, Arizona State Forestry Division 2013). These events are not limited to the United States. For example, in 2010, 44 police and firefighters were entrapped and ultimately perished in the 2010 Mount Carmel Fire in Israel (United Nations Office for the Coordination of Humanitarian Affairs 2010).

Gleason (1991) proposed a system of interdependent safety measures to reduce firefighter risk of burnover and entrapment: lookouts, communications, escape routes, and safety zones (LCES). Safety zones are a critical component of this system, essentially areas large enough to allow firefighters to escape the harmful effects of fire (Beighley 1995). According to the US National Wildfire Coordinating Group (NWCG) Incident Response Pocket Guide (IRPG), LCES should be established and known to all members of a fire crew before it is needed (NWCG 2014). The IRPG indicates that safety zones can be areas that have already burned, can be natural (rock areas, water, meadows) or constructed (clear-cuts, roads, helicopter landing zones), and should be scouted for size and hazards. If they are upslope of flames, downwind of flames, or adjacent to particularly heavy fuels, a larger safety zone is needed (National Wildfire Coordinating Group 2014).

Safety zones must be large enough to hold firefighting personnel and equipment, and should provide a safe separation distance (SSD) between vegetation and these

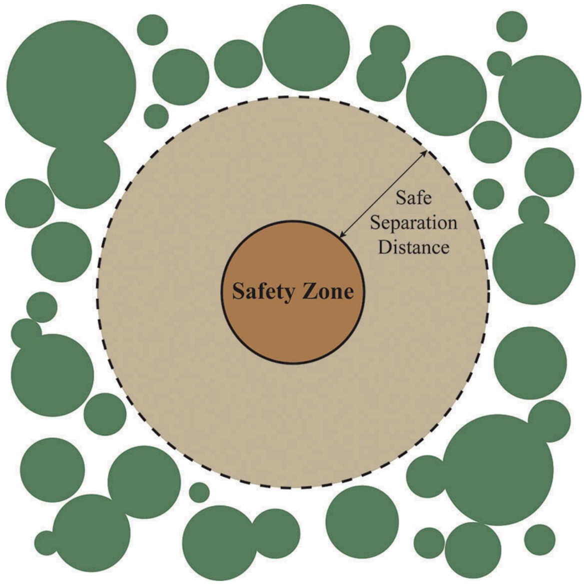

Figure 2. Basic safety zone example diagram (after Dennison *et al.* 2014).

assets (Figure 2). The SSD must be large enough that heat from the wildfire is reduced to the point that a fire shelter is not necessary to prevent firefighter injury. The current NWCG guideline for estimating SSD comes from Butler and Cohen (1998a), who determined, based on radiant heat modeling, that SSD should be equal to or greater than four times flame height. This guideline assumes flat terrain and does not account for convective heat transfer, which can strongly contribute to firefighter heat exposure (Butler 2014, Butler *et al.* 2015).

Relatively few studies have attempted to characterize convective heat flux in a wildland fire environment, due to its inherent complexity and measurement difficulty. Frankman *et al.* (2013) demonstrated the varied but significant effects of convective energy flux (both heating and cooling), which were heavily influenced by fuel, wind, and terrain conditions. Zarate *et al.* (2008) suggested adding a 20% increase in SSD to account for the additional convective heat flux. Butler *et al.* (2015) point out that exposure to high winds and adjacency to steep slopes has the potential to transfer convective heat as far as two to three flame lengths ahead of the fire front. To account for convective heat flux, Butler (2015) proposed that the SSD calculation can be adjusted using a 'slope-wind factor' (Δ):

$$\mathrm{SSD} = 8 \times H_v \times \Delta, \tag{1}$$

where H_v is vegetation height. For flat terrain and low wind speeds, SSD is simply eight times vegetation height, identical to the current NWCG guideline (assuming flame height is equal to two times the vegetation height). Although flame height will not always be equal to twice the vegetation height, it is a useful approximation for crown fire conditions, enabling a broad-scale pre-fire assessment of SSD based on existing vegetation conditions, rather than requiring that firefighters predict flame heights. As slope and wind speed increase, the slope-wind factor increases to provide a larger SSD

Table 1. Slope-wind factor safe separation distance matrix from Butler (2015).

	Slope-wind factor (Δ)			
	Slope (%)			
Wind speed (ms^{-1})	Flat (<20%)	21–30%	31–50%	>50%
Light (0–3)	1	1	3	5
Moderate (4–7)	1.5	2	4	6
Strong (8–13)	3	3	6	7.5
Very strong (>13)	4.5	5	7	9

value. Examples of slope-wind factors from Butler (2015) are shown in Table 1. Based on the slope-wind factor, a potential safety zone sufficient for flat terrain and moderate wind speed (SSD = $8 \times H_v \times 1.5$) could be too small for flat terrain and strong wind speed (SSD = $8 \times H_v \times 3$).

Field estimates of safety zone geometry and surrounding vegetation height, which are used to calculate SSD, are prone to large errors (Bechtold *et al*. 1998, Steele 2000). This study demonstrates a method for identifying, evaluating and mapping the relative suitability of all potential safety zones throughout a given area in order to improve the process of safety zone designation. Specifically, the objectives of this study are (1) to introduce a new metric for evaluating potential safety zones, based on safety zone geometry, area, surrounding vegetation height, and number of firefighting personnel present: the Safe Separation Distance Score (SSDS), (2) to develop an algorithm to map SSDS using lidar data, and (3) to test the implementation of the algorithm on a lidar dataset from Tahoe National Forest.

2 Methods

2.1 *Data and study area*

Lidar is a type of active remote-sensing system that enables the generation of very high spatial resolution three-dimensional models of terrain and above-ground structure (vegetation, buildings, etc.) (Lefsky *et al*. 2002). Discrete return lidar instruments, which are typically mounted on an aircraft, emit hundreds of thousands of individual pulses of laser light to the ground every second. The light in each pulse interacts with features on the ground and reflects back to the sensor. Extremely accurate measurement of the elapsed time between light transmission and reception enables calculation of a precise elevation of the reflective object (Lefsky *et al*. 2002). The result of such data collection is typically a point cloud comprised of millions of points, each with an associated *x*, *y*, and *z* value. In order to be able to extract useful information from a lidar point cloud, points are generally classified into ground and non-ground (e.g. vegetation and buildings) (Meng *et al*. 2010). Many methods exist for ground point classification, the accuracies of which vary significantly according to the method used, the terrain conditions and the degree to which surface features obscure the ground surface (Reutebuch *et al*. 2003). Discrete ground points can be interpolated into digital terrain models (DTMs), which are continuous raster representations of the ground surface (Kraus and Pfeifer 2001). In the presence of vegetation, lidar pulses typically interact with several surfaces prior to reaching the ground surface. In these cases, the 'last return' can often, though not always, represent the ground surface, while the 'first return' represents the elevation of the highest reflective surface. First return points can be interpolated to generate a digital surface model (DSM). In the absence of above-ground objects (e.g. bare soil), surface and terrain model pixel values should be equal. Vegetation height can be computed by subtracting terrain elevations from surface elevations (Dubayah and Drake 2000, Popescu *et al*. 2002). Dennison *et al*. (2014) used lidar to map safety zones for different expected flame heights, but did not directly utilize variable vegetation height information provided by lidar data.

SSDS were calculated for potential safety zones within Tahoe National Forest, California, USA. A lidar-derived DTM and DSM, each with a spatial resolution of 1.0 m, were obtained from the US Forest Service (Figure 3). The raw point cloud data from which these datasets were derived were collected between 2013 and 2014 with an average pulse density of 8 pulses/m^2.

The study area encompasses 5335 km^2, 4549 km^2 (85%) of which is within the Tahoe National Forest administrative boundary. There is a wide range of elevations throughout the study area, from 268 m at its lowest point to 2813 m at the highest with a mean elevation of 1686 m. The land cover is primarily composed of conifer forest (77%), shrubland (8%), riparian vegetation (4%), sparse vegetation (3%), hardwood forest (2%), and grassland (1%), with the remaining area being a combination of a variety of rarer cover types, including developed land (LANDFIRE 2012). Within the dominant conifer class, the distribution of forest types is as follows: Douglas-fir (*Pseudostuga menziesii*)/grand fir (*Abies grandis*)/white fir (*Abies concolor*) mix (34%), red fir (*Abies magnifica*) (28%)/Douglas-fir (*Pseudotsuga*

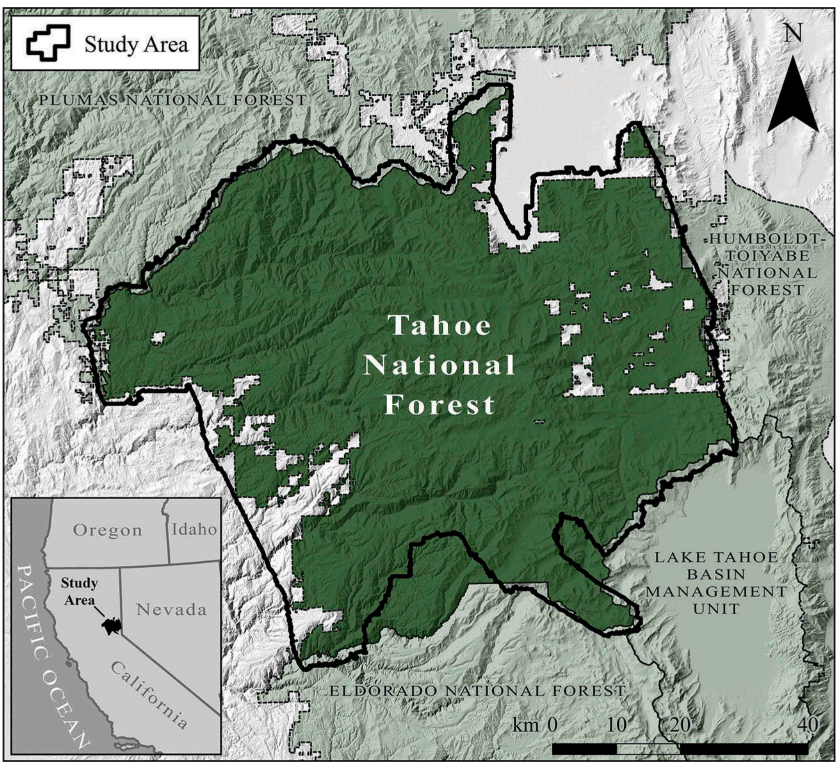

Figure 3. Study area map.

menziesii)/ponderosa pine (*Pinus ponderosa*)/lodgepole pine (*Pinus contorta*) mix (21%), ponderosa pine (*Pinus ponderosa*) (15%), and other conifer (2%).

2.2 *Safety zone model*

SSDS is a unitless value that is attributed to a forest clearing that provides firefighting personnel with an estimate of the relative suitability of that clearing as a safety zone according to its area, geometry, surrounding vegetation height, and number of firefighting personnel and equipment present. SSDS can be compared directly to the slope-wind factor for expected wind speed and slope (Table 1) to determine whether a specific safety zone is adequate for expected conditions. Using lidar data, an SSDS can be calculated for all potential safety zones within an area. Multiple geospatial data processing steps are required to calculate SSDS from a lidar-derived terrain and surface models. An automated model was developed in Python using primarily ESRI ArcGIS tools to facilitate the safety zone analysis across a relatively large study area with many forest clearings varying in size, shape, and surrounding vegetation conditions. This section describes, in detail, the model workflow.

In order to be able to assess vegetation height, a canopy height model (CHM) was generated by subtracting the terrain elevation from the surface elevation for each pixel (x,y), such that:

$$\mathrm{CHM}_{(x,y)} = \mathrm{DSM}_{(x,y)} - \mathrm{DTM}_{(x,y)}, \tag{2}$$

where DSM is the digital surface model and DTM is the digital terrain model. The resulting raster dataset contained a pixel-based representation of height, in meters, above the ground surface (Figure 4(a)). In order to locate forest clearings, a tree/non-tree map was generated using a simple height threshold classification, wherein all CHM values less than 1 m in height were classified as 'non-tree' and all CHM values equal to or greater than 1 m in height were classified as 'tree'. A kernel filtering process was then applied to the tree/non-tree classification to eliminate small and/or isolated trees that would be unlikely, in a wildfire setting, to have sufficient connectivity to surrounding fuels to negatively affect the quality of an otherwise open area as a safety zone (Dennison *et al*. 2014). A 10% threshold within a circular kernel 30 m in diameter was used for filtering. If the area classified as 'tree' was less than 10% of the 30 m kernel, it was reclassified to 'non-tree'. Both the diameter of the kernel and the percent threshold are important parameters of the model that have direct impacts on the resultant classification of clearings versus treed areas, but for the purposes of this study, no sensitivity tests were performed to determine their relative effects on resulting safety zone maps.

Clearings were located by buffering the 'tree' pixels by 8 m and identifying those areas remaining beyond the extent of the buffers. Eight meters was used because in a best-case scenario (low wind, low slope, 1 m tall surrounding trees), the safe separation distance would be 8 m (8 × 1 m × 1). Clearings were then buffered back to the forest edge by 8 m, in order to represent the full extent of the clearing. Figure 4(b) illustrates one such clearing, though it should be noted that (Figure 4), as a whole, illustrates a single example of processes performed on nearly 86,000 clearings throughout the study area.

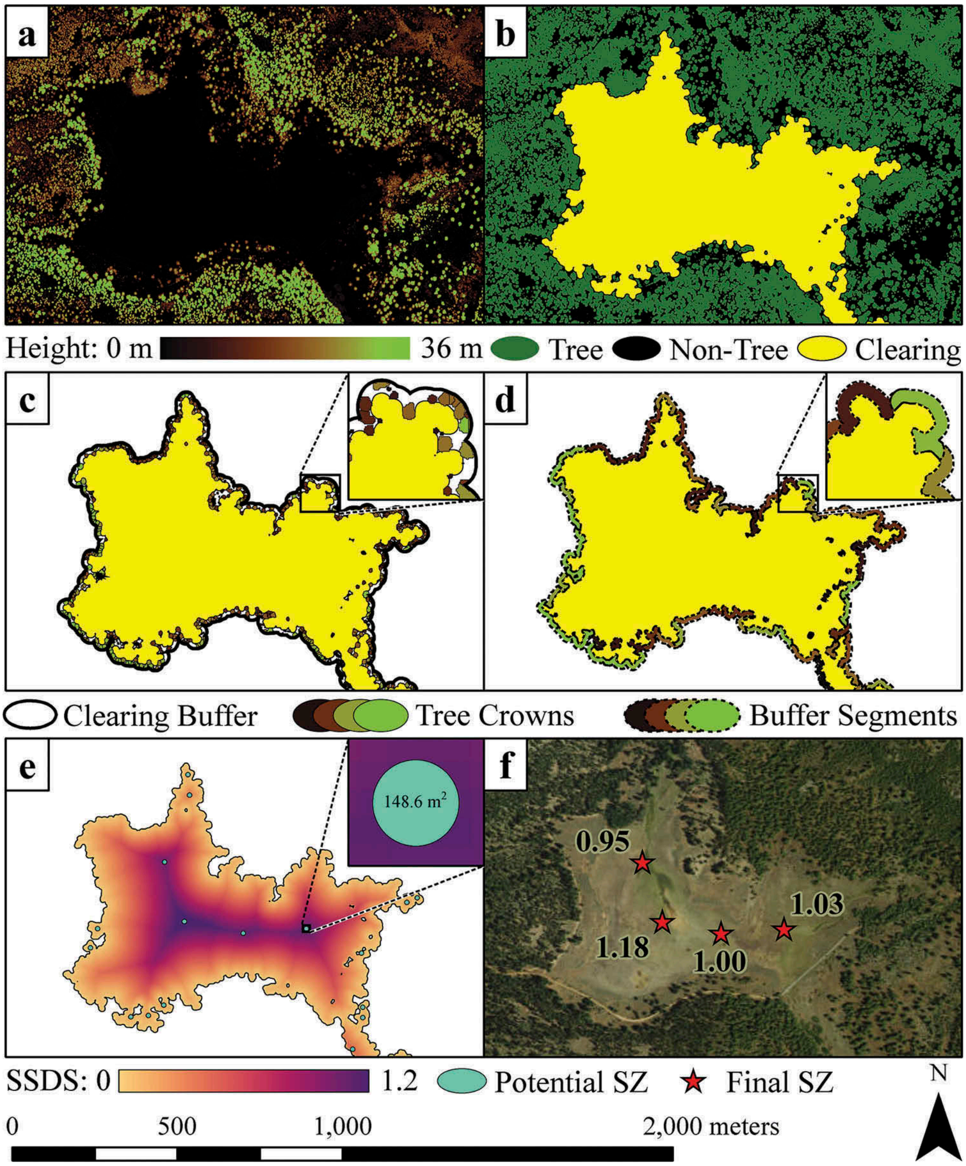

Figure 4. Model workflow from canopy height model (a) to clearing classification (b), surrounding tree crown delineation and height calculation (c), segment-based mean surrounding vegetation height calculation (d), pixel-based SSDS calculation and safety zone placement (e), and safety zone SSDS result (f).

For each individual clearing, the following steps were performed. In the interest of assessing the vegetation immediately surrounding the clearing, a 10 m buffer was created around it. The CHM was then clipped to the extent of this buffer area and surrounding tree crowns were delineated individually using a watershed segmentation technique first introduced by Wang *et al.* (2004). Figure 5 graphically depicts this technique. Beginning with a CHM, all non-tree pixels (height <1 m) were removed and

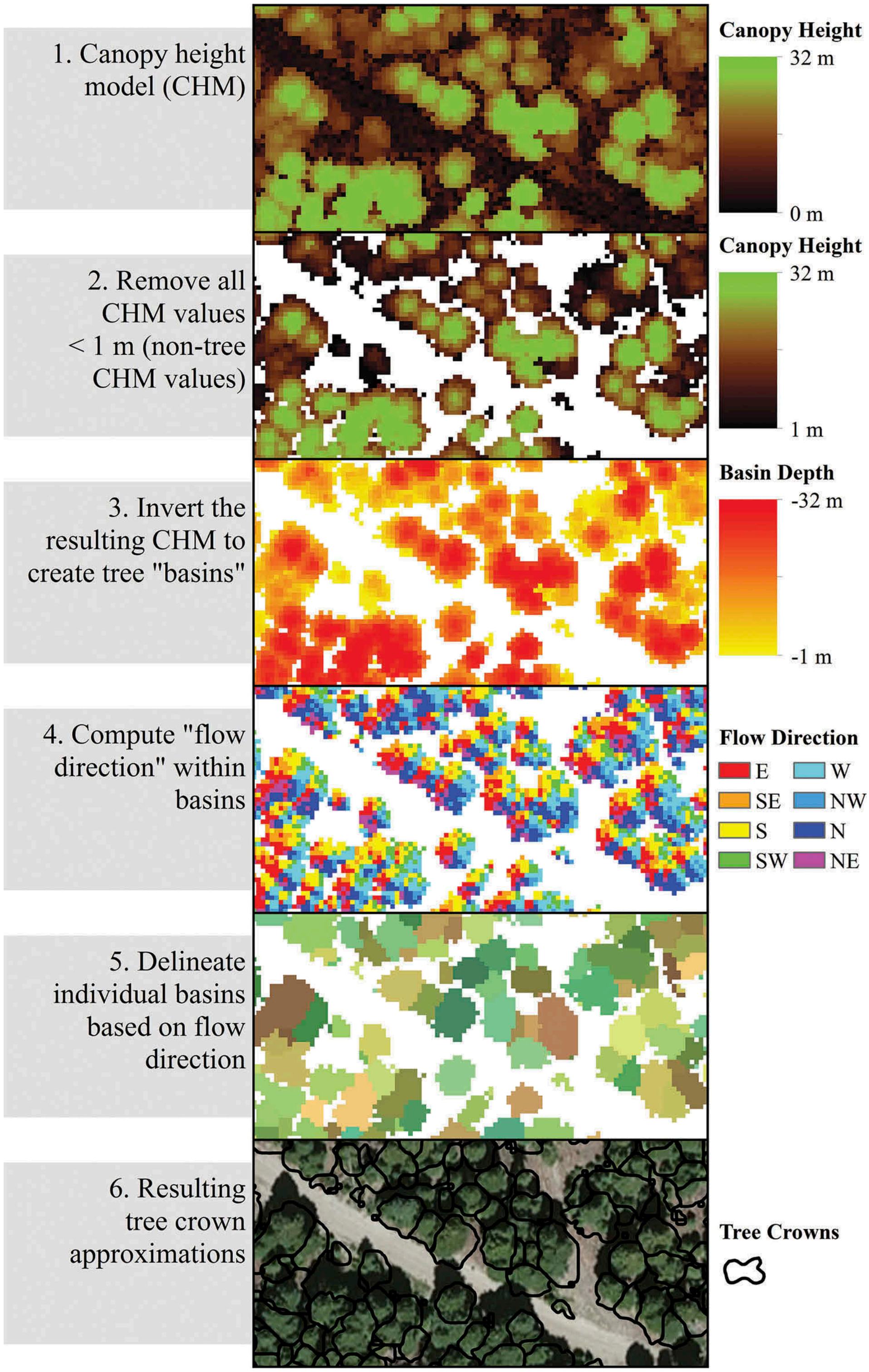

Figure 5. Tree crown delineation method.

the resulting raster was inverted (multiplied by −1) to create tree 'basins' out of what were previously tree peaks. A 'flow direction' image was then generated which simulates the flow of water within each of these tree basins. Because these basins all drain internally (because, in reality, each tree comes to an individual peak), we then delineate individual basins, or watersheds, which generate a raster approximation of individual tree crowns. These tree crowns are then converted to a vector polygon for further analysis.

Tree crown polygons were used to calculate individual tree heights by computing a within-polygon maximum CHM value. As Figure 4(c) highlights, the result of this process was an array of polygons surrounding the clearing, each of which has an associated height. However, to analyze the effect of each individual tree height on SSD would be extremely processing-intensive, rendering an algorithm such as this ineffective for application on a broad scale. On the other hand, to compute a single mean surrounding vegetation height for an entire clearing would be an over-generalization, particularly for large clearings where surrounding vegetation heights can vary significantly from one portion of their perimeter to another. This variability in vegetation height is important to capture, as it will have direct impacts on where the safety zone should be located within a clearing (further from areas with taller vegetation, closer to areas with shorter vegetation). Thus, mean surrounding vegetation height was calculated within each of a series of buffer segments, each 10 m wide and roughly 100 m in length, surrounding each clearing (Figure 4(d)). Mean tree height was weighted by tree crown area to avoid the downward-bias resulting from the likely presence of a greater number of smaller (and shorter) trees than larger (and taller) trees, such that:

$$H_{\mathrm{v}} = \frac{\sum_{i=1}^{n} a_i \times h_i}{\sum_{i=1}^{n} a_i}, \tag{3}$$

where a is crown area and h is height for each individual tree crown i. For each linear buffer, Euclidean distance from surrounding vegetation was then calculated on a continuous pixel basis within the clearing. Using mean vegetation height and distance from surrounding vegetation for each pixel (x,y) within the clearing, a pixel-based $\mathrm{SSDS}_{(x,y)}$ was calculated, such that:

$$\mathrm{SSDS}_{(x,y)} = \frac{\mathrm{ED}_{(x,y)}}{(8 \times H_{\mathrm{v}})}, \tag{4}$$

where $\mathrm{ED}_{(x,y)}$ is the Euclidean distance from vegetation raster data for each pixel (x,y). This SSDS calculation is essentially a transformation of the proposed SSD equation (Equation (1)), substituting the Euclidean distance raster data for SSD and solving for Δ on a pixel-by-pixel basis, thus making SSDS and Δ directly comparable values. As a result of this calculation, each clearing had a series of individual SSDS raster layers, each associated with one of the linear buffers surrounding the clearing. A single clearing-wide SSDS raster is then generated by computing a pixel-by-pixel minimum SSDS value among each of the contributing SSDS rasters.

Most often the clearings that emerged from this mapping process were irregularly-shaped, unlike the simplified case illustrated in (Figure 2). Figure 4 highlights one such irregular clearing. Though it maintained non-tree connectivity throughout the clearing, its large size and irregular shape could enable the placement of multiple safety zones within. From a geospatial standpoint, one can clearly see in Figure 4(e) how there are several local maxima of SSDS within the clearing due to the effects of clearing geometry and variable surrounding vegetation height. In order to address this we employed another watershed-based approach for locating safety zones within the clearing. This involved taking the inverse of the SSDS raster (multiplying SSDS by −1 to form SSDS 'basins'), calculating 'flow direction', and locating 'sinks', or areas of internal drainage, the results of which represent the points of local maximum SSDS, or the safest points within each distinct portion of the clearing (Figure 4(e)).

The last critical variable addressed in this model is firefighter crew size. Safety zones need to be large enough to accommodate both personnel and equipment (e.g. engines). Andrews (2009) suggests 4.6 m^2 (50 ft^2) is required for each crew member and 27.9 m^2 (300 ft^2) is required for each engine. For the purpose of this study, an assumed crew size of 20 firefighters and 2 engines was used, requiring a minimum safety zone area of 148.6 m^2. Circular areas of this size, representing potential safety zones where firefighters and equipment would assemble, were centered on the points of local maximum SSDS (Figure 4(e)). Rather than use this highest SSDS to represent the entire safety zone, however, the lowest within-safety zone SSDS is used, because this represents the relative safety of the zone on its outside edge. Again, because SSDS values are directly comparable to Δ values, we can determine that, because the lowest possible Δ is 1, then any safety zone with an SSDS <1 will be unsuitable in any wind and terrain conditions. Thus, all potential safety zones with an SSDS much less than 1 are eliminated from consideration. However, given the continuous nature of SSDS, one could still identify perhaps sub-optimal but still viable safety zones with SSDS of 0.9 or 0.95, if these are the only options available to a fire crew, as seen in (Figure 4(f)).

Finally, a slope raster dataset is calculated throughout the entire study area using the lidar-derived DTM. Mean slope is then computed within each safety zone. The resulting safety zone polygons each have an associated SSDS and slope written to the attribute table. Since SSDS is derived directly from the proposed SSD equation, SSDS values can then be queried and compared to the Δ values in the slope-wind factor matrix to determine the relative suitability of that clearing as a potential safety zone. For example, if a safety zone has an SSDS of 1.5, it is suitable in all conditions where a Δ of 1.5 or less is required.

3 Results

The resulting map of potential safety zones with associated SSDS values (greater than 1) throughout the study area can be seen in Figure 6. As the map highlights, there are relatively few safety zones that have an SSDS of 1 or greater, which is to say that at the time of lidar acquisition, the vegetation conditions found within the study area would offer relatively few potential safety zones that are sufficiently large in even the best-case (low wind and low slope) scenarios. Clustering of potential safety zones is clearly evident, particularly in the northeastern portion of the study area. Much of the vegetation in this area was burned in the high severity Cottonwood fire in 1994. Although roughly 20 years passed between the Cottonwood fire and the lidar data acquisition, the

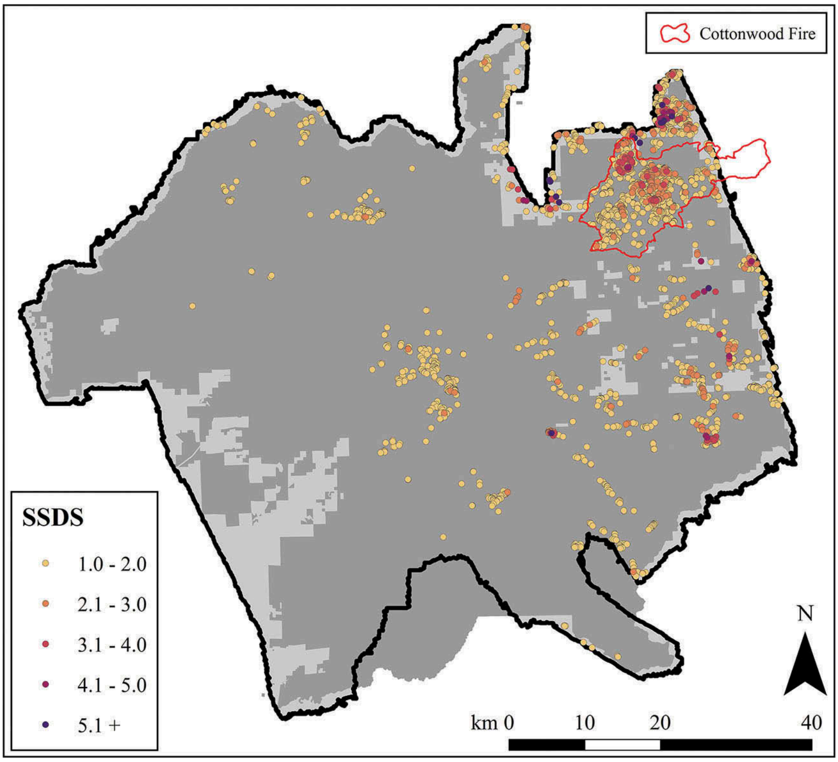

Figure 6. Potential safety zones with associated safe separation distance score values throughout the study area. The area burned by the 1994 Cottonwood fire is outlined in red.

subsequent slow regeneration of vegetation in certain areas of the fire lends itself well to use as potential safety zones, according to the results of our model. Potential safety zones are particularly sparse in the southern and western portions of the study area, where continuous swaths of forest, 400 km^2 or greater in area, are entirely devoid of potential safety zones even at the lowest recommended SSDS of 1. It should be noted that many of the largest safety zones with the highest SSDS values are lakes. While lakes may seem like an ideal safety zone (no slope, vegetation, or possibility of burning), they present their own set of risks, such as drowning or hypothermia (Butler 2014). The resulting safety zones were compared to the USGS National Hydrography Dataset, and all of those that fell within a waterbody were removed.

Table 2 provides a tabular account of the number of potentially viable safety zones in each combination of wind speed and slope according to resulting SSDS. It stands to reason

Table 2. Number of suitable safety zones in each combination of wind speed and slope according to SSDS values.

	Slope (%)			
Wind speed (ms^{-1})	Flat (<20%)	21–30%	31–50%	>50%
Light (0–3)	2367	2367	99	15
Moderate (4–7)	881	352	30	7
Strong (8–13)	99	99	7	2
Very strong (>13)	19	15	2	2

that there are many more potential safety zones with low SSDS, suitable in low wind-flat slope conditions, than high SSDSs, suitable in high wind-steep slope conditions, simply because there are many more small forest clearings than large. With that said, there are still only a total of 2367 potential safety zones with scores of greater than or equal to 1 throughout the entire study area. When comparing SSDS values to the slope-wind factor matrix, we see that a safety zone with an SSDS of 1 would be suitable in the lowest wind and slope conditions (<3 ms^{-1} and <30%, respectively). However, as wind speeds and slopes increase, higher SSDS values are needed to render a safety zone viable. For example, if wind speeds are slightly higher (4–7 ms^{-1}), and slopes remain less than 30%, an SSDS of at least 2 is needed, of which there are a total of 352. The highest SSDS value found throughout the study area was 9.65, which would be suitable for any combination of wind speed and slope.

Given that slope is a static landscape variable, SSDS can be compared to slope in order to determine the wind speed conditions in which a given safety zone would be viable. When comparing safety zone slopes to SSDS values, we see that even at the lowest wind speed category (<3 ms^{-1}), there are only 1547 potentially suitable safety zones (Figure 7). As wind speed increases to 4–7, 8–13, and greater than 13 ms^{-1}, the number of safety zones drops to 500, 79, and 14, respectively.

Perhaps equally important to the number of potential safety zones is their spatial distribution, which directly impacts accessibility. As stated earlier, there is a clearly non-random distribution of safety zones throughout the study area, leaving vast tracts of forested land without any viable safety zones, particularly in the southwest. Figure 8 depicts distance intervals and associated approximate travel times to safety zones with varying SSDS thresholds. Travel rates were assumed to be 1.4 ms^{-1}, an empirically derived average hiking rate along flat slopes from Tobler (1993). Table 3 highlights the proportions of the study area that fall within these same distance and time intervals from safety zones. In low wind-low slope scenarios, where an SSDS of at least 1 is needed, roughly 8% of the study area is within a 5-minute hike to the nearest safety zone, 17% within 10 min, 41% within 30 min, and 64% within an hour (Figure 8, Table 3). Conversely, with high-SSDS safety zones being so sparse throughout the study area, only 1% of the area is within an hour of the nearest safety zone with SSDS ≥7.

Clearing area is the best predictor of SSDS. Given that most forest clearings contain several potential safety zones, we performed a linear regression between the SSDS of the highest-rated safety zone within each clearing and the clearing area. As the data were heavily right-skewed, we used a reciprocal-square transformation for the SSDS data and a log transformation for the area data (Figure 9). The relatively low predictive power that emerged (r^2 = 0.38) is due to the fact that clearing geometry and surrounding vegetation height also have significant impacts on a given safety zone's SSDS. Additional geometric parameters such as clearing perimeter and area-to-perimeter ratio were also tested for statistical relationships, but their predictive powers were lower (r^2 = 0.32 and r^2 = 0.28, respectively).

4 Discussion and conclusions

This study introduced a new metric and geospatial model for identifying and evaluating potential wildland firefighter safety zones using lidar data. Lidar proves to be an excellent resource for assessing many of the most important predictors of safety zone quality: clearing size and geometry, within- and surrounding-clearing vegetation height,

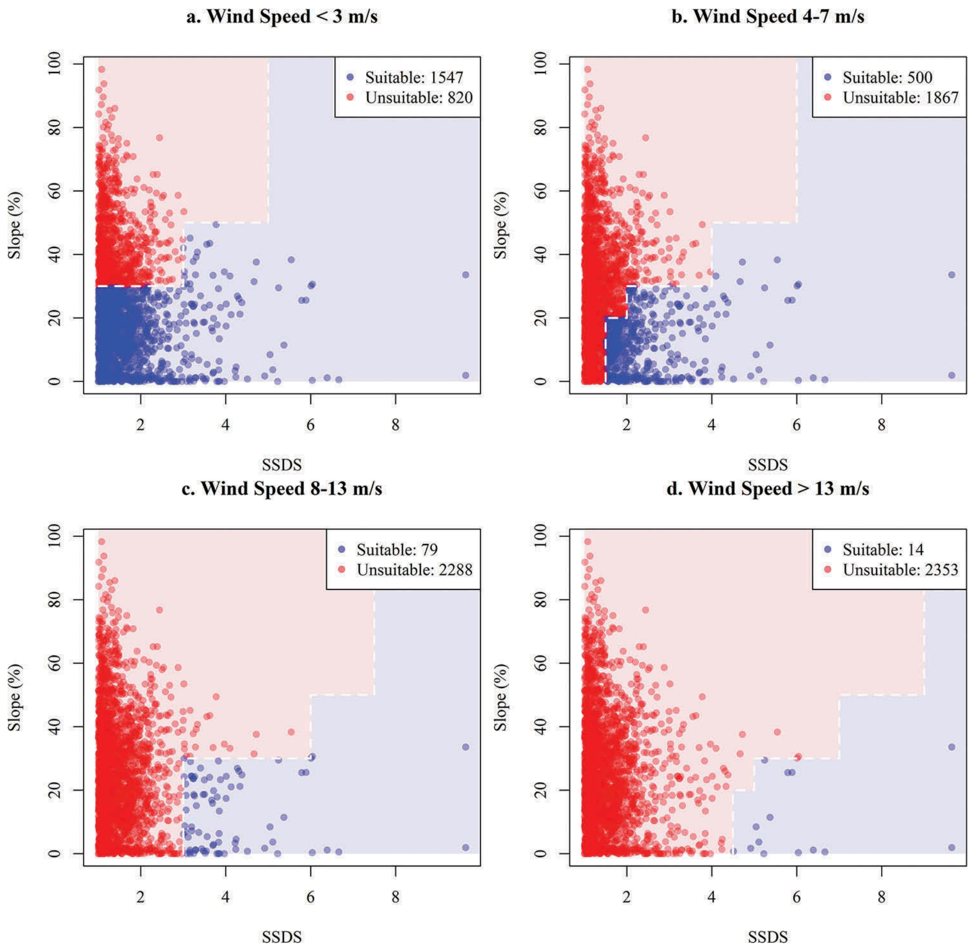

Figure 7. Scatterplots of safety zone SSDS values compared to slopes broken down by wind speed category. The blue and red regions represent areas of suitability and unsuitability, respectively, according to slope and wind conditions as defined by the slope-wind factor matrix (Table 1).

and slope. However, at present, safety zones are evaluated and designated on the ground by firefighting personnel with limited influence of geospatial information. The use of a standardized metric (SSDS) evaluated through a robust, automated computer model, such as was introduced in this study, stands to greatly increase the reliability and consistency with which safety zones are evaluated. Instead of relying on visual interpretation of safety zone area, geometry and surrounding vegetation height for each individual potential safety zone visited on the ground, the SSDS model provides firefighters with a map of all of the potential safety zones in the surrounding area, each of which is attributed with a value that can be used to determine the wind and terrain conditions in which a given safety zone will be suitable. It should be clearly noted, however, that this methodology is not a replacement of ground-based safety zone evaluation. Like any model-based remote-sensing analysis, ground verification is essential. Unlike most other remote-sensing analyses, ground verification is particularly important in this study, given the potentially dangerous and even fatal consequences

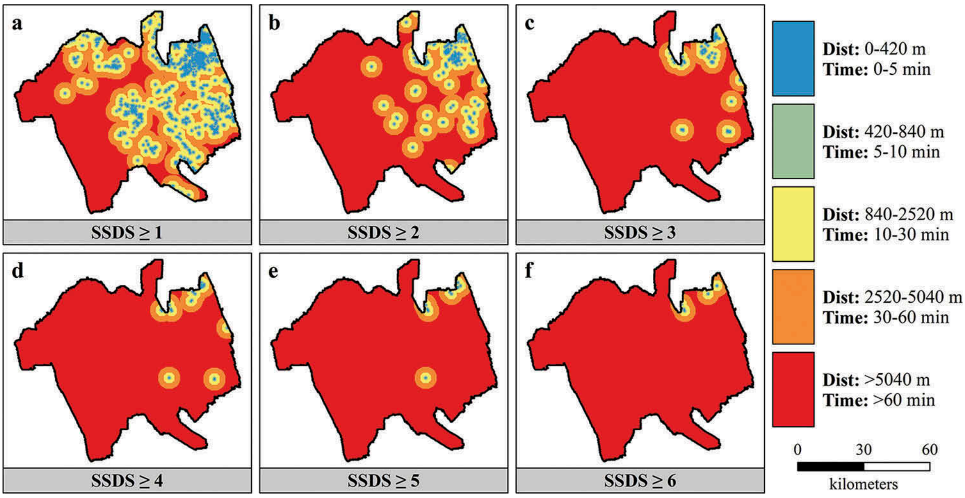

Figure 8. Euclidean distance and estimated travel time to nearest potential safety zone at a range of SSDS thresholds throughout the study area.

Table 3. Percent of study area within distance and travel time of safety zones with different SSDS thresholds.

Distance	0–420 m	420–840 m	840–2520 m	2520–5040 m	>5040 m
Time:	0–5 min	5–10 min	10–30 min	30–60 min	>60 min
SSDS ≥1	8.11%	8.69%	23.94%	23.65%	35.61%
SSDS ≥2	1.84%	2.57%	9.57%	18.06%	67.95%
SSDS ≥3	0.67%	1.07%	3.53%	7.71%	87.02%
SSDS ≥4	0.25%	0.48%	2.28%	5.82%	91.17%
SSDS ≥5	0.13%	0.31%	1.28%	3.34%	94.94%
SSDS ≥6	0.06%	0.17%	0.94%	2.29%	96.54%
SSDS ≥7	0.01%	0.04%	0.29%	0.85%	98.80%
SSDS ≥8	0.01%	0.04%	0.29%	0.85%	98.80%
SSDS ≥9	0.01%	0.04%	0.29%	0.85%	98.80%

of utilizing an unsuitable safety zone. However, whereas under the existing protocol for safety zone identification, all potential safety zones must be visited and verified, the method we have presented will enable a more targeted approach, eliminating the need to visit areas the model has determined that no viable safety zones exist, according to surrounding vegetation, clearing geometry, slope, wind, and crew size. This will greatly increase the efficiency of safety zone selection and minimize potential for selecting unsuitable sites.

The results of the model implementation in Tahoe National Forest highlight a relative sparseness of suitable safety zones, especially for high winds and steep slopes. Particularly in the western and southern portions of the study area, if a wildfire were to occur, safety zones (at least those composed of existing forest clearings) are few and far between. However, knowing where safety zones are *not* may be just as useful as knowing where safety zones are. In the event of a wildfire in an area devoid of natural safety zones, this model can be used to highlight areas where safety zones could be created through the use of controlled burning, timber harvesting or other manipulation of existing fuels, or through the utilization of recently burned areas in a wildfire. If

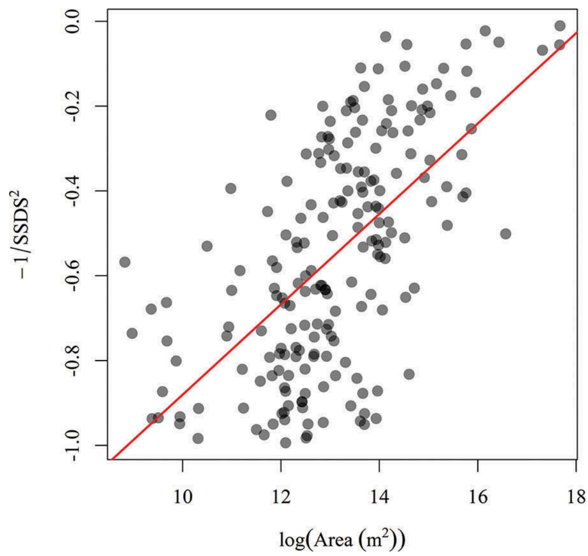

Figure 9. Linear regression between safety zone SSDS and clearing area in which the safety zone fell.

creation or enlargement of safety zones in not feasible then fire management tactics should be modified to reduce firefighter risk, such as standing down until conditions change or the fire moves to a more suitable location. Similarly, if an area has an existing potential safety zone, but the SSDS is too low for the slope and wind conditions, it could provide an impetus to expand the safety zone to a suitable size and/or geometry.

One of the most important parameters not addressed by this model is fuel type, both within and surrounding the potential safety zone. The model, in its present form, makes a key assumption that vegetation less than 1 m in height is 'non-tree', and therefore eligible to become a safety zone, provided other conditions are met. While the 1 m threshold is a model parameter that can be manipulated, regardless of vegetation height, certain fuel types are undesirable for safety zones. For example, shrubs may be short in stature but highly flammable and might not provide a viable safety zone without treatment. Although we are only taking advantage of lidar's ability to characterize vegetation height in this study, lidar can be further exploited for the estimation of other fuel parameters, such as crown bulk density and canopy base height (Andersen *et al.* 2005). Another potential solution to this issue is incorporation with additional remote-sensing data. The use of hyperspectral imagery, for example, could be used to characterize within-safety zone fuel conditions through the spectral unmixing of green vegetation, non-photosynthetic vegetation and soils (Roberts *et al.* 2006). Alternatively, in the absence of hyperspectral image availability, tools such as LANDFIRE can provide critical fuel information such as vegetation type, height and cover, and fire behavior fuel models, albeit at a coarser level of thematic precision and with limited accuracy (Rollins 2009). Additionally, it is understood that fuel type and condition of the vegetation surrounding the safety zone will impact the relative flammability of this vegetation, potential for crown fire, and fire intensity. In order to eventually incorporate such information into SSDS, more detailed studies on the specific relationships between fuel and fire parameters are needed.

Another key variable not assessed in the implementation of this algorithm is safety zone accessibility. A large safety zone completely devoid of flammable vegetation may be evaluated as having a very high SSDS, suggesting suitability in a wide range of wind and terrain conditions, but if it is not accessible by a fire crew, it is not a viable option. Escape routes are a critical component of fire safety, representing pre-defined pathways for accessing safety zones (NWCG 2016). Given the similarities between the conditions that define the relative suitability of escape routes and safety zones (low slope, low vegetation cover), similar lidar-based approaches can be used in the future for determining optimal escape routes from fire crew location to a safety zone.

A key limitation to the practical application of this study and widespread use of the proposed model for safety zone evaluation, at present, is the lack of lidar data availability throughout most of the United States. In order to obtain a reliable picture of safety zones on a broad scale, there needs to be a similarly reliable lidar dataset extending into all areas where wildfires can occur. With the USGS 3D Elevation Program underway (Snyder 2012), a nationwide map of safety zones could be generated and provided to land management and firefighting agencies. However, at the time of writing, with the expected completion of a nationwide lidar dataset still several years in the future, a more targeted approach to lidar data collection in fire-prone areas can provide critical information for supporting firefighter safety operations in the interim. Alternatively, in the absence of lidar data there are other options that could prove viable, such as stereo imagery-based pseudo-point cloud extraction. However, a key limitation with stereo imagery methods is the absence of a reliable ground surface model in areas with dense tree canopies, thus limiting the ability to extract tree heights which are a critical parameter in safety zone analysis (St-Onge *et al*. 2008). Another related limitation is the fact that lidar represents a single snapshot in time. Particularly in fire-prone areas, vegetation is a dynamic entity that changes with the presence of disturbance events including wildfire, timber harvesting, insect and disease outbreaks, major wind events, and, over a much longer timescale, climate change. By one account (National Fire Protection Association 2011), as much as 90% of safety zones are designated 'in the black' – in already-burned areas. These areas would obviously not be depicted in a safety zone map created using lidar data flown prior to the wildfire event. One possible solution to this is the incorporation of unmanned aerial vehicular technology. The model as it is being presented in this study is intended to be a tool for pre-fire planning (O'Connor *et al*. 2016), though it is conceivable that this methodology could be adapted to a rapid response tool used for a more targeted approach for safety zone identification and evaluation. Alternatively, the use of predictive vegetation growth models and fuel accumulation curves could be used to estimate vegetation conditions following disturbance events to fill in temporal gaps in lidar data collections and/or to highlight areas to target repeat lidar data collection efforts.

Finally, it is worth noting that the scientific basis of convective and radiant heat transfer modeling upon which Δ and, as a result, SSDS are based, still requires further study (Finney *et al*. 2013, 2015). As stated earlier, particularly convective heat transfer is a tremendously challenging physical phenomenon to model in a controlled environment. While the data used in this study are based on recent findings in the research of radiant and convective heat transfer in wildfires and their effects on humans, more research is needed. Specifically, a more nuanced understanding of the effects of specific vegetation types and fuel conditions, which can both be approximated with remote sensing, on heat transfer would greatly improve the effectiveness of implementing our algorithm. That being said, even if the specific *Δ* and SSDS numbers were to be updated with newer science, the core methodology presented in this study would remain a viable option for increasing firefighter safety.

Acknowledgments

Funding for this research was provided by the US Forest Service National Fire Plan through the Office of Research, the NWCG Fire Behavior Subcommittee, and the Wildland Fire Management Research Development & Application Program, Cooperative Agreements 14JV11221637123 and 15CR11221637105. We would like to thank the Forest Service Region 5 Remote Sensing Lab, Carlos Ramirez, Scott Conway, and Kirk Evans for providing lidar products for Tahoe National Forest. Finally, we would like to thank the anonymous reviewers, whose thoughtful questions and comments helped to improve this paper.

Disclosure statement

No potential conflict of interest was reported by the authors.

Funding

Funding for this research was provided by the US Forest Service National Fire Plan through the Office of Research, the NWCG Fire Behavior Subcommittee, and the Wildland Fire Management Research Development & Application Program, Cooperative Agreements 14JV11221637123 and 15CR11221637105.

References

Andersen, H.-E., McGaughey, R.J., and Reutebuch, S.E., 2005. Estimating forest canopy fuel parameters using LIDAR data. *Remote Sensing of Environment*, 94, 441–449. doi:10.1016/j.rse.2004.10.013

Andrews, P.L., 2009. BehavePlus fire modeling system, version 5.0: variables. *General technical report RMRS-GTR-213WWW revised*. Department of Agriculture, Forest Service, Rocky Mountain Research Station, Fort Collins, CO.

Arizona State Forestry Division. *Yarnell hill fire: serious accident investigation report*. 23 September 2013 [online]. Available from: http://wildfiretoday.com/documents/Yarnell_Hill_Fire_report.pdf [Accessed 10 July 2016].

Bechtold, W.A., Zarnoch, S.J., and Burkman, W.G., 1998. Comparisons of modeled height predictions to ocular height estimates. *Southern Journal of Applied Forestry*, 22 (4), 216–221.

Beighley, M., 1995. Beyond the safety zone: creating a margin of safety. *Fire Management Notes*, 55 (4), 22–24.

Butler, B.W., *et al*., 1998. Fire behavior associated with the 1994 South Canyon fire on storm king mountain, CO. *USDA forest service research paper RMRSRP-9*. Rocky Mountain Research Station, Fort Collins, CO.

Butler, B.W., 2014. Wildland firefighter safety zones: a review of past science and summary of future needs. *International Journal of Wildland Fire*, 23, 295–308. doi:10.1071/WF13021

Butler, B.W., 2015. Firefighter safety zones [online]. *Fire, fuel, and smoke science program, USDA forest service rocky mountain research station*. Available from: http://www.firelab.org/project/firefighter-safety-zones [Accessed 30 July 2016].

Butler, B.W. and Cohen, J.D., 1998a. Firefighter safety zones: a theoretical model based on radiative heating. *International Journal of Wildland Fire*, 8 (2), 73–77. doi:10.1071/WF9980073

Butler, B.W. and Cohen, J.D., 1998b. Firefighter safety zones: how big is big enough? *Fire Management Notes*, 58, 13–16.

Butler, B.W., Parsons, R., and Mell, W., 2015. *Recent findings relating to firefighter safety zones*. Missoula: U.S. Department of Agriculture, Forest Service, Rocky Mountain Research Station, 30–34.

Dennison, P.E., Fryer, G.K., and Cova, T.J., 2014. Identification of firefighter safety zones using lidar. *Environmental Modelling & Software*, 59, 91–97. doi:10.1016/j.envsoft.2014.05.017

Dubayah, R.O. and Drake, J.B., 2000. Lidar remote sensing for forestry. *Journal of Forestry*, 98 (6), 44–46.

Finney, M.A., *et al*., 2013. On the need for a theory of wildland fire spread. *International Journal of Wildland Fire*, 22, 25–36. doi:10.1071/WF11117

Finney, M.A., *et al*., 2015. Role of buoyant flame dynamics in wildfire spread. *Proceedings of the National Academy of Sciences*, 112 (32), 9833–9838. doi:10.1073/pnas.1504498112

Frankman, D., *et al*., 2013. Measurements of convective and radiative heating in wildland fires. *International Journal of Wildland Fire*, 22 (2), 157–167. doi:10.1071/WF11097

Gleason, P., 1991. LCES – a key to safety in the wildland fire environment. *Fire Management Notes*, 52 (4), 9.

Kraus, K. and Pfeifer, N., 2001. Advanced DTM generation from lidar data. *International Archives of Photogrammetry Remote Sensing and Spatial Information Sciences*, 34 (3/W4), 23–30.

LANDFIRE, 2012. Existing vegetation type layer, LANDFIRE 1.3.0 [online]. *US department of the interior, geological survey*. Available from: http://landfire.cr.usgs.gov/viewer/[Accessed 10 July 2016].

Lefsky, M.A., *et al*., 2002. Lidar remote sensing for ecosystem studies lidar, an emerging remote sensing technology that directly measures the three-dimensional distribution of plant canopies, can accurately estimate vegetation structural attributes and should be of particular interest to forest, landscape, and global ecologists. *BioScience*, 52 (1), 19–30.

Meng, X., Currit, N., and Zhao, K., 2010. Ground filtering algorithms for airborne lidar data: a review of critical issues. *Remote Sensing*, 2 (3), 833–860. doi:10.3390/rs2030833

National Fire Protection Agency, 2011. *Firewise communities: firefighter safety in the WUI [online]*. Available from: http://learningcenter.firewise.org/Firefighter-Safety/3-4.ph. [Accessed 4 January 2016].

National Interagency Fire Center, 2016. *Wildland fire fatalities by year [online]*. Available from: https://www.nifc.gov/safety/safety_documents/Fatalities-by-Year.pdf [Accessed 4 January 2016].

National Wildfire Coordinating Group, 2014. *Incident response pocket guide [online]*. Available from: http://www.nwcg.gov/sites/default/files/products/pms461.pdf [Accessed 4 January 2016].

National Wildfire Coordinating Group, 2016. *Glossary A-Z [online]*. Available from: http://www.nwcg.gov/glossary/a-z [Accessed 4 January 2016].

O'Connor, C.D., *et al*., 2016. Getting ahead of the wildfire problem: quantifying and mapping management challenges and opportunities. *Geosciences*, 6 (35), 1–18. doi:10.3390/geosciences6030035

Popescu, S.C., Wynne, R.H., and Nelson, R.F., 2002. Estimating plot-level tree heights with lidar: local filtering with a canopy-height based variable window size. *Computers and Electronics in Agriculture*, 37, 71–95. doi:10.1016/S0168-1699(02)00121-7

Reutebuch, S.E., *et al*., 2003. Accuracy of a high-resolution lidar terrain model under a conifer forest canopy. *Canadian Journal of Remote Sensing*, 29 (5), 527–535. doi:10.5589/m03-022

Roberts, D.A., *et al*., 2006. Evaluation of Airborne Visible/Infrared imaging Spectrometer (AVIRIS) and Moderate Resolution Imaging Spectrometer (MODIS) measures of live fuel moisture and fuel condition in a shrubland ecosystem in southern California. *Journal of Geophysical Research*, 111, 1–16. doi:10.1029/2005JG000113

Rollins, M.G., 2009. LANDFIRE: a nationally consistent vegetation, wildland fire, and fuel assessment. *International Journal of Wildland Fire*, 18 (3), 235–249. doi:10.1071/WF08088

Snyder, G.I., 2012. *The 3D elevation program: summary of program direction* [online]. US Department of the Interior, US Geological Survey. Available from: https://pubs.usgs.gov/fs/2012/3089/pdf/fs2012-3089.pdf [Accessed 14 December 2016].

Steele, J., 2000. Effective firefighter safety zone size: a perception of firefighter safety. *4th International wildland fire safety summit*, Edmonton, AB, CA: International Association of Wildland Fire, 171–177.

St-Onge, B., *et al*., 2008. Mapping canopy height using a combination of digital stereo-photogrammetry and lidar. *International Journal of Remote Sensing*, 29 (11), 3343–3364. doi:10.1080/01431160701469040

Tobler, W., 1993. *Three presentations on geographical analysis and modeling, Technical Report 93-1*. Santa Barbara: National Center for Geographic Information and Analysis, University of California.

United National Office for the Coordination of Humanitarian Affairs. *Israel Carmel fire situation report #2*. 6 December 2010 [online]. Available from: http://reliefweb.int/sites/reliefweb.int/files/resources/DD3E82B287DB17CD852577F1006E883B-Full_Report.pdf [Accessed 10 July 2016].

Wang, L., Gong, P., and Biging, G.S., 2004. Individual tree-crown delineation and treetop detection in high-spatial-resolution aerial imagery. *Photogrammetric Engineering & Remote Sensing*, 70 (3), 351–357. doi:10.14358/PERS.70.3.351

Zarate, L., Arnaldos, J., and Casal, J., 2008. Establishing safety distances for wildland fires. *Fire Safety Journal*, 43 (8), 565–575. doi:10.1016/j.firesaf.2008.01.001